



HAL
open science

Pyramid wavefront sensor Optical Gains compensation using a convolutional model

Vincent Chambouleyron, Olivier Fauvarque, Pierre Janin-Potiron, Carlos Correia, Jean-François Sauvage, Noah Schwartz, Benoît Neichel, Thierry Fusco

► **To cite this version:**

Vincent Chambouleyron, Olivier Fauvarque, Pierre Janin-Potiron, Carlos Correia, Jean-François Sauvage, et al.. Pyramid wavefront sensor Optical Gains compensation using a convolutional model. In press. hal-02776372v1

HAL Id: hal-02776372

<https://hal.science/hal-02776372v1>

Preprint submitted on 4 Jun 2020 (v1), last revised 2 Dec 2020 (v2)

HAL is a multi-disciplinary open access archive for the deposit and dissemination of scientific research documents, whether they are published or not. The documents may come from teaching and research institutions in France or abroad, or from public or private research centers.

L'archive ouverte pluridisciplinaire **HAL**, est destinée au dépôt et à la diffusion de documents scientifiques de niveau recherche, publiés ou non, émanant des établissements d'enseignement et de recherche français ou étrangers, des laboratoires publics ou privés.

Pyramid wavefront sensor Optical Gains compensation using a convolutional model

V. Chambouleyron^{1,2}, O. Fauvarque^{1,3}, P. Janin-Potiron^{2,1}, C. Correia⁴, J-F. Sauvage^{2,1}, N. Schwartz⁵, B. Neichel¹, and T. Fusco^{2,1}

(Affiliations can be found after the references)

February 28, 2020

ABSTRACT

Context. Extremely Large Telescopes have chosen the Pyramid wavefront sensor (PyWFS) over the more widely used Shack-Hartmann WaveFront Sensor (SHWFS) to perform their Single Conjugate Adaptive Optics (SCAO) mode. The PyWFS is a Fourier-filtering based sensor, which has proven to be strongly efficient for astronomical purposes. However, it shows non-linearity behaviors that lead to a reduction of its sensitivity when working around a non-null phase. This effect, called Optical Gains (OG), degrades the performance of the closed loop and prevents accurate correction of Non-Common-Path Aberrations (NCPA).

Aims. We aim at computing these so-called OG with a fast and agile technique in order to control the PyWFS measurements for adaptive optics closed-loop systems.

Methods. Thanks to a new theoretical description of the PyWFS, which uses a convolutional model to describe the sensor, we analytically predict the behavior of the PyWFS in closed-loop operation. This model allows us to explore the impact of residual phases on the properties of the PyWFS measurements in terms of sensitivity, and associated OG. The proposed method relies on the knowledge of the residual phase statistics and allows to automatically estimate the current OG. End-to-End numerical simulations are used to validate our predictions and test the relevance of our approach.

Results. We show that an accurate estimation of the OGs is possible by only using the AO telemetry data to derive statistical information of the turbulence. The method is then fully non-invasive. We further show that by only having an estimation of the current Fried parameter r_0 and the basic system characteristics, OGs can be estimated within 10% accuracy. The proposed method applies to Pyramid WFS, but also to any Fourier-Filtering WFS suffering from OG variations.

Key words. Adaptive Optics – Pyramid Wavefront Sensor – Optical Gains – Convolutional Model

1. Introduction

The PyWFS is an optical device used to perform wavefront sensing proposed for the first time in 1996 (Ragazzoni 1996). Inspired by the Foucault knife test, the PyWFS is a pupil plane wavefront sensor performing optical Fourier filtering thanks to a glass pyramid located at the focal plane (see figure 1). This pyramid splits the electromagnetic (EM) field in four beams producing four different filtered images of the entrance pupil. This filtering operation allows the conversion of phase information at the entrance pupil into amplitude at a pupil plane where a quadratic sensor is used to record the signal. The PyWFS usually includes an additional optical module called a modulation mirror, which, by moving the Point-Spread Function (PSF) around the tip of the pyramid, allows to increase the linearity range of the device at the expense of its sensitivity.

This wavefront sensor shows higher sensitivity than the SHWFS and is therefore a key element for present and future AO systems (Neichel et al. 2016; Davies et al. 2018). Its complexity and the limited knowledge on the nature of the PyWFS measurements led to extensive studies of this device (Vérinaud 2004; Guyon 2005; Hutterer et al. 2018). One of the most complete study of this wavefront sensor is a model describing the sensor as a convolutional system described by its three main properties (Fauvarque et al. 2019): the shape of the pyramid mask m , the modulation function w , and the entrance pupil geometry \mathbb{I}_p (see figure 2). This model is called the **convolutional model**, and al-

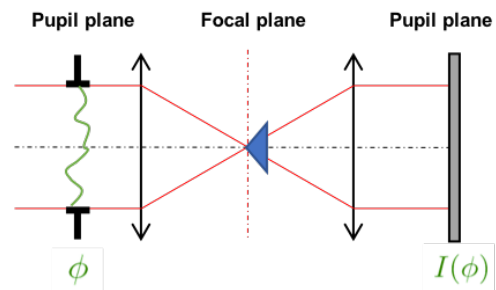


Fig. 1. The PyWFS is a Fourier filtering wavefront sensor. A pyramidal mask is placed at a focal plane in order to achieve optical filtering. The intensities $I(\phi)$ recorded on the detector show a relationship to the entrance phase ϕ .

lows one to compute a simple quantity which fully describes the behaviour of the sensor: its impulse response given equation 1.

$$\mathbf{IR} = 2\text{Im}(\widehat{m}(\widehat{m} \star \widehat{w}\mathbb{I}_p)) \quad (1)$$

where $\widehat{\cdot}$ is the Fourier transform operator and \star the convolution symbol.

Now that the PyWFS has captured the interest of AO scientists, one of its major limitations needs to be handled: its strong non-linear behaviour which leads to a spatial frequency-dependent loss of sensitivity during on-sky operations. This loss of sensitivity can be encoded in a quantity called Optical Gains

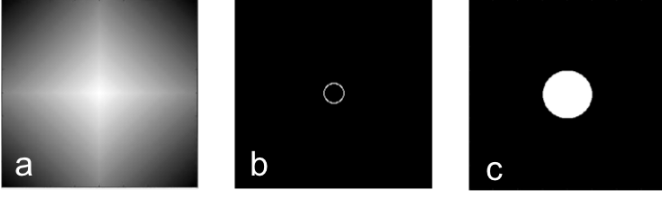


Fig. 2. **a:** $arg(m)$ - shape of the pyramid mask. **b:** w - modulation function. **c:** I_p - pupil shape.

(OG) (Korkiakoski et al. 2008). Tracking these OG during on-sky operations has therefore become one of the key priorities to fully control PyWFS measurements. The spatial error due to OG can be dominated by other terms in the error budget, but it becomes predominant in case of bad seeing conditions and/or when pointing at extended objects. In closed loop operation, OG and temporal gains can be merged so there is only one global gain to optimize for each mode. There are now new and robust strategies that can make possible such an optimization (Deo et al. 2019) but they don't allow to disentangle OG from the loop temporal gains. However, the knowledge of OG alone is still crucial for Non-Common Path Aberrations (NCPA) handling which is emerging as a critical step in wavefront control for PyWFS based systems (Esposito et al. 2015). It is also a key issue in order to properly analyze loop telemetry data for PSF reconstruction. The objective of this paper is to present a new strategy based on a physical description of the PyWFS to compute quickly and accurately these OG, independently from the loop temporal gains.

In section 2, we propose to present a clear definition of the OG and how we can better understand the nature of OG which are generated by residual phases on the PyWFS. In section 3, we then show that it is possible to use the convolutional model approach to accurately compute OG, providing we have some statistical knowledge of the shape of the residual phases.

2. Definition of Optical Gains and application to PyWFS in presence of residual phases

2.1. The interaction matrix approach as a linear model of the PyWFS

The wavefront sensor is described by a matrix which fully encodes the linear behaviour of the system. This so-called Interaction Matrix (IM) is computed through a calibration process by recording the slopes of the linear responses of the wavefront sensor to a set of phases ϕ_i which forms a basis of the phase space we want to control. For each mode, the slope of the linear response $\delta I_{calib}(\phi_i)$ can be computed through the following operation, called "push-pull" operation:

$$\delta I_{calib}(\phi_i) = \frac{I_{calib}(a\phi_i) - I_{calib}(-a\phi_i)}{2a} \quad (2)$$

where I_{calib} is the intensities recorded on the wavefront sensor camera and a is the amplitude of the mode used for calibration. This amplitude a should be as small as possible in order to stay within the linear regime. But in reality, we want it to be large enough so the signal-to-noise ratio of the measurement is satisfactory while staying in the linearity zone. This maximization of signal-to-noise ratio during calibration can be helped by using optimal calibration strategies, such as the Hadamard approach (Meimon et al. 2015). The interaction matrix computed during the calibration process IM_{calib} is then the concatenation

the slopes recorded for all modes.

$$IM_{calib} = (\delta I_{calib}(\phi_1), \dots, \delta I_{calib}(\phi_i), \dots, \delta I_{calib}(\phi_N)) \quad (3)$$

In the well-known inverse problems framework, this calibration step is actually a way to compute the **linear forward operator** of our system, linking the phase to the pyramid measurements.

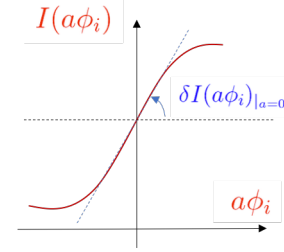


Fig. 3. Sketch of the PyWFS response curve for a given mode ϕ_i . The push-pull method around a null-phase consists in computing the slope of this curve for $a = 0$.

2.2. The Optical Gains: an offset between calibration regime and sensing regime

IM_{calib} is computed in a specific regime that we call the *calibration regime*. The framework used for the rest of the paper is the following: we suppose the calibration is done with a point-like source around a flat wavefront (no reference phase) and for a given modulation radius.

During operation - which we call the *sensing regime* - the wavefront sensor differs inevitably from the calibration regime, if nothing else because we can't reach the perfect diffraction limit of the telescope. Because of the non-linear nature of the PyWFS, this leads to a change in the behaviour of the sensor. These non-linearities can be handled by considering the PyWFS as a sensor with a varying linear behaviour which depend on the sensing regime. We therefore make the hypothesis that the sensor's behaviour in the sensing regime can be described by an IM that we call $IM_{sensing}$ and in that case the linear behaviour has to be measured again to have the accurate description of the direct problem.

$$\delta I_{sensing}(\phi_i) = \frac{I_{sensing}(a\phi_i) - I_{sensing}(-a\phi_i)}{2a} \quad (4)$$

When the PyWFS is working around a non-null reference phase, we have the following relationship:

$$I_{sensing}(a\phi_i) = I_{calib}(a\phi_i + \phi_{ref}) \quad (5)$$

because of PyWFS non-linear behaviour, we have $I_{calib}(a\phi_i + \phi_{ref}) \neq I_{calib}(a\phi_i) + I_{calib}(\phi_{ref})$ and therefore:

$$\begin{aligned} \delta I_{sensing}(\phi_i) &= \frac{I_{sensing}(a\phi_i) - I_{sensing}(-a\phi_i)}{2a} \\ &= \frac{I_{calib}(a\phi_i + \phi_{ref}) - I_{calib}(-a\phi_i + \phi_{ref})}{2a} \\ &\neq \delta I_{calib}(\phi_i) \end{aligned} \quad (6)$$

which naturally leads to offsets between IM_{calib} and $IM_{sensing}$.

We define the **optical transfer matrix** T_{opt} as the transfer matrix describing the offsets between the sensing regime and the calibration regime. This matrix is a square matrix of size $N_{\text{modes}} \times N_{\text{modes}}$.

$$IM_{\text{sensing}} = IM_{\text{calib}} \cdot T_{\text{opt}} \quad (7)$$

In order to obtain the correct linear description of our sensor for a given sensing regime, we therefore need to correct the interaction matrix computed during calibration by the optical transfer matrix.

From the equation above, we can write the exact definition of the optical transfer matrix:

$$T_{\text{opt}} = IM_{\text{calib}}^{\dagger} \cdot IM_{\text{sensing}} \quad (8)$$

2.3. Diagonal approximation and OG definition in the PyWFS measurement space

An approximation can strongly simplify the computation of T_{opt} : the **diagonal approximation**. This approximation consists in assuming that T_{opt} is a diagonal matrix (Deo et al. 2019). That is to say there is no cross-talk between modes when we are switching from the calibration regime to the sensing regime. In other words, the slope of the linear behaviour for each mode ϕ_i is increased or reduced by a scalar factor $G(\phi_i)$ called the modal OG.

In the case of the diagonal approximation, we can define the modal OG $G(\phi_i)$ without having to use the pseudo inverse $IM_{\text{calib}}^{\dagger}$ (which depends on the conditioning): we propose to use the usual scalar product $\langle \cdot | \cdot \rangle$ defined in the measurement space to compare $\delta I_{\text{sensing}}(\phi_i)$ and $\delta I_{\text{calib}}(\phi_i)$ for each mode ϕ_i .

$$G(\phi_i) = \frac{\langle \delta I_{\text{sensing}}(\phi_i) | \delta I_{\text{calib}}(\phi_i) \rangle}{\langle \delta I_{\text{calib}}(\phi_i) | \delta I_{\text{calib}}(\phi_i) \rangle} \quad (9)$$

$\langle \delta I_{\text{sensing}}(\phi_i) | \delta I_{\text{calib}}(\phi_i) \rangle$ represents the projection of the measurement in the sensing regime onto the measurement in the calibration regime and $\langle \delta I_{\text{calib}}(\phi_i) | \delta I_{\text{calib}}(\phi_i) \rangle$ is a normalization term. The definition of OG given here differs slightly from the ones previously given in the literature (Korkiakoski et al. 2008; Deo et al. 2019) and has the advantage of being independent of the reconstructor: this is a description in the measurement space only. An equivalent formulation of equation 9 in terms of matrices is the following:

$$G_{\text{opt}} = \frac{\text{diag}({}^t IM_{\text{sensing}} \cdot IM_{\text{calib}})}{\text{diag}({}^t IM_{\text{calib}} \cdot IM_{\text{calib}})} \quad (10)$$

where G_{opt} is a vector containing all the $G(\phi_i)$ for $i \in [1, N_{\text{modes}}]$.

2.4. Optical Gains induced by residual phases

In this subsection, we aim at understanding the nature of OG induced by residual phases. We can describe residual phases ϕ_{residual} as an offset point around which we estimate the different modes ϕ_i . However, we still consider a calibration done with a point-like source with a flat wavefront. We can therefore write:

$$I_{\text{sensing}}(a\phi_i) = I_{\text{calib}}(a\phi_i + \phi_{\text{residual}}) \quad (11)$$

Besides, this offset point changes at each measurement because ϕ_{residual} is a dynamic quantity. That is to say that IM_{sensing} is changing at each iteration, depending on the shape of ϕ_{residual} . Although it seems hard to determine the state of IM_{sensing} at each instant, we can find a way to compute the **averaged state** of the sensing regime $\langle IM_{\text{sensing}} \rangle_t$ which gathers $\langle \delta I_{\text{sensing}}(\phi_i) \rangle_t$ for each mode.

$$\langle IM_{\text{sensing}} \rangle_t = (\langle \delta I_{\text{sensing}}(\phi_1) \rangle_t, \dots, \langle \delta I_{\text{sensing}}(\phi_i) \rangle_t, \dots, \langle \delta I_{\text{sensing}}(\phi_N) \rangle_t) \quad (12)$$

In this regard, we rely on the convolutional formalism of the PyWFS proposed by Fauvarque et al. (2019). Within the framework of this model, it is possible to compute an analytic formula to take into account the impact of residual phases on the PyWFS measurements: the sensing regime is then described by a PyWFS for which the modulation function (see equation 1) is changed according to this formula:

$$w \leftarrow w \star e^{-\frac{1}{2} D_{\phi_{\text{res}}}} \quad (13)$$

This equation gives a fundamental insight on PyWFS measurements in presence of residual phases: it was well-known that residual phases act as an extra modulation that lowers the pyramid sensitivity. We now know how to quantify this loss: the impact depends on residual phases statistics through the structure function, and therefore through the Power Spectral Density (PSD) of the residual phases. It is then possible to define its new impulse response in the averaged sensing regime assuming isotropy and stationarity of the residual phases:

$$IR_{\text{sensing}} = 2\text{Im}(\tilde{m}(\hat{m} \star \widehat{w}|_p e^{-\frac{1}{2} D_{\phi_{\text{res}}}})) \quad (14)$$

The reader must notice that in this equation, the modulation function is the only quantity that is affected. This means that the impact of residual phases can be described as a collection of tip-tilt offsets during one measurement: the residual phase OG are thus depicted as a sort of incoherent offsets. Going from an apparently coherent offset to an incoherent offset in the nature of these OG comes from the time averaging operation. This in fact is very well understood in the image formation field through the derivation of the transfer function of the atmosphere Roddier (1981): by averaging over time, we can find an analytic formula for a long-exposure seeing limited PSF, which can not be only described by a coherent phase aberration in the pupil plane.

In this section, we have exposed a new measurement space based definition of OG and explained how they naturally emerge from PyWFS non-linearities when working with offset between calibration and sensing regime. In the following part, we propose a new method based on the convolutional model to perform a fast and accurate computation of these OG.

3. A new strategy to compute PyWFS modal Optical Gains through the convolutive model

3.1. Convolutional formalism: a path to optical Gains computation

In case of OG due to residual phases, the diagonal approximation ensures that the knowledge of the diagonal elements of G_{opt} is enough to compute IM_{sensing} . The expression of $G(\phi_i)$ given equation 9 can be written within the convolutional model using

the impulse responses of the calibration regime and the sensing regime:

$$G_{\text{conv}}(\phi_i) = \frac{\langle \mathbf{IR}_{\text{sensing}} \star \phi_i | \mathbf{IR}_{\text{calib}} \star \phi_i \rangle}{\langle \mathbf{IR}_{\text{calib}} \star \phi_i | \mathbf{IR}_{\text{calib}} \star \phi_i \rangle} \quad (15)$$

Thus, we have a way to compute the modal OG thanks to the convolutional model, knowing the following system parameters: the shape of the mask m , the modulation function w , the pupil shape \mathbb{I}_p , and the structure function of the residual phases $D_{\phi_{\text{res}}}$. In order to identify whether the convolutional model used here is accurate enough to allow a good estimation of the modal OG - *i.e* whether $G_{\text{conv}}(\phi_i)$ is close to $G(\phi_i)$ or not - we compared the predictions of the model with End-to-End simulations. The results of this study are presented in the next section.

3.2. Convolutional model versus End-to-End simulations

The End-to-End simulations are performed using the *OOMA*O MATLAB toolbox (Conan & Correia 2014), considering a **8 m class telescope**. The resolution in the pupil diameter is 90 pixels. We use a Karhunen-Loève basis of 400 modes on which we compute all our interaction matrices and OG. The wavefront sensing is done in the visible ($\lambda = 550 \text{ nm}$).

Sensitivity curves

We use the convolutional model to retrieve the well-known sensitivity curves of the PyWFS where the sensor behaves as a slope sensor for the frequencies lower than the modulation radius and as a phase sensor for the frequency above it. For the chosen system configuration, we present figure 4 results for two different modulation radii. We remind the reader that for each mode, the sensitivity is given by:

$$s(\phi_i) = \|\delta I_{\text{calib}}(\phi_i)\|_2 = \sqrt{\langle \delta I_{\text{calib}}(\phi_i) | \delta I_{\text{calib}}(\phi_i) \rangle} \quad (16)$$

We note a small offset between the model and the end-to-end simulations for the low-order modes. This can be explained by the hypothesis of the sliding pupil used for the derivation of the convolutional model. This issue was tackled in Fauvarque et al. (2019).

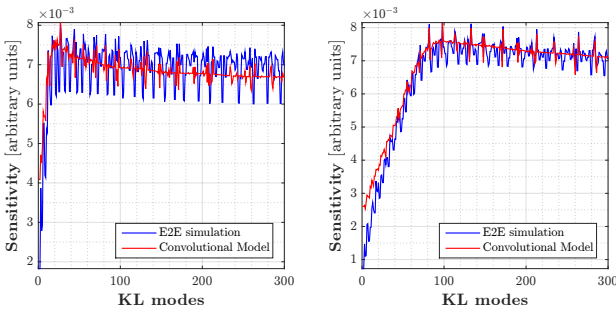


Fig. 4. The well-known pyramid sensitivity curves. **Left:** Modulation radius $r_{\text{mod}} = 2\lambda/D$. **Right:** Modulation radius $r_{\text{mod}} = 5\lambda/D$.

Modal Optical Gains

We carry out the study by computing modal OG through End-to-End simulations in different system configurations and we then

compare to the ones predicted through the convolutional model. We suppose here that we know the statistics of the turbulence. In other words, we have access to the PSD (Power Spectral Density) or the structure function of the residual phases. We will focus on how to get this data in a practical way later in this paper.

End-to-End simulations - We proceed in the following way: given a PSD, we generate 20 decorrelated phases. We then compute the interaction matrices IM_{sensing} around each of these phases (using a push-pull method) and we use the formula 10 to compute the OG. The averaged values for each different PSD chosen are presented figure 5 and figure 6 (the shaded areas represent the maximum and minimum values found for the OG for 20 phase realisations).

Convolutional Model - We use exploit the same PSD used for the End-to-End simulations to compute the $\mathbf{IR}_{\text{sensing}}$ equation 14 and we retrieve the OG thanks to equation 15.

We can define two main PSD configurations around which we can compute the OG:

- The full turbulence OG: in that case, the PyWFS works in open-loop and the wavefront sensing is done on a seeing-limited EM field at the tip of the pyramid. In the vast majority of systems, this case is verified at the very first iterations when we close the loop. After a few closed-loop iterations, the EM field seen by the pyramid is no longer seeing-limited because we are in closed-loop operation. We then fall in the second configuration described below. Tracking and compensating the OG in this case can be interesting when the system has trouble to bootstrap on a strong turbulence or when we want to close the loop for lower modulation radii. The results of the comparison for this configuration are given figure 5: we note the strong agreement between the convolutional model and the End-to-End simulations.
- The residual phases OG: the Adaptive Optic loop is closed and the OG are due to imperfect correction of the wavefront. This case is the most interesting one because it can allow us to enhance the closed-loop performance. For this setting, the results are given figure 6: we still have a strong match between our model and the End-to-End simulations.

By testing our model for different system configurations (different modulation radii, different r_0 , open or closed loop residual phases) we have demonstrated that the convolutional model can be used to predict the OG with sufficient accuracy to remain in their statistical variability range. It therefore provides a fast and agile way to track OG, providing knowledge of the residual PSD. In the next section, we hence focus on how to get this data in a practical way.

3.3. How to get the residual PSD?

We suggest here to obtain the residual PSD from the telemetry data. It is a non-invasive method which is already deeply investigated in the PSF reconstruction field (Beltramo-Martin et al. 2019). To achieve this goal, we generally also rely on the commands sent to the DM. The process works in two steps:

- If we record the integrated commands sent to the DM, we can assess the shape of the turbulence: we will be able to get the Fried parameter r_0 and therefore have an estimation of the PSD shape outside the correction zone. The estimation of r_0 thanks to the telemetry is usually not perfectly accurate

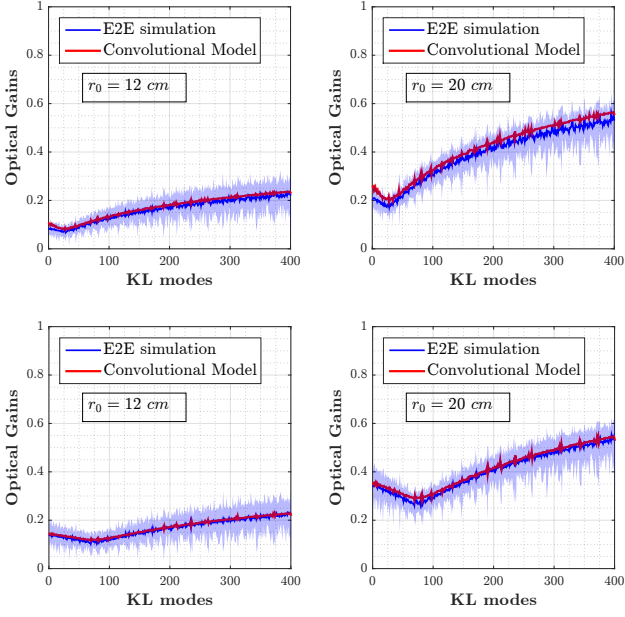


Fig. 5. OG computed on full turbulence screens for different r_0 . The convolutional model fits well with the OG computed by E2E simulations. The shaded area represents the maximum and minimum values found for the OG for 20 phase realisations. The modulation radius is $r_{mod} = 3\lambda/D$.

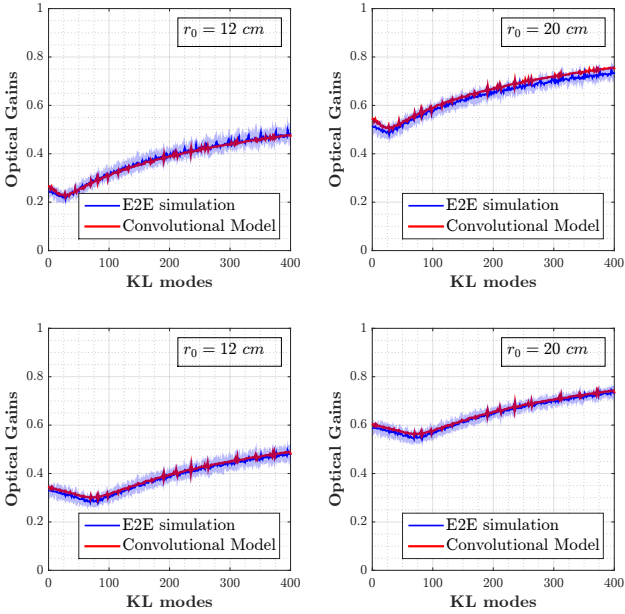


Fig. 6. OG for closed loop residual phases. Number of actuators in the pupil: 20. **Top:** $r_{mod} = 3\lambda/D$. **Bottom:** $r_{mod} = 5\lambda/D$.

and the Fried parameter is often overestimated. However, it has been shown that an AO system can be well characterized in order to correct for this offset (Fétick et al. 2019).

- Checking the residual commands will give us an information on the residual PSD inside the correction zone. This method is not ideal, because all the commands sent to the DM are already tainted by the OG problem. This problem can be overcome by using models describing the analytical PSD inside the correction zone, providing a simple set of parameters describing the system (Rigaut et al. 1998).

We therefore need to know what level of accuracy is required when computing the residual phases PSD through telemetry data and with the help of an analytical model of our system. Using the convolutional model, we propose a brief study to analyse the contribution of the different parts of residual PSD on the **OG morphology**. As we mentioned earlier, we can split the contribution of the residual phases into two parts: the fitting PSD and the PSD inside correction zone. It is therefore interesting to study the OG for each of these contributors.

For that purpose we choose two system configurations: a 8m telescope given a $r_0 = 15\text{ cm}$ with either 20 actuators (NAOS configuration on the VLT) or 40 actuators within the same pupil diameter (SPHERE configuration on the VLT: Beuzit et al. (2019)). We use a typical residual PSD of these systems to compute the OG thanks to the convolutional model. Figure 7, we show results when the OG are computed for the full PSD, for the fitting part of the PSD and for the PSD inside the correction area only. It is clear that OG gains are dominated by the energy which lies in the fitting PSD, even for the high-contrast configuration (40×40 actuators in the pupil). We can conclude that the OG morphology is mainly constrained by the Fried parameter r_0 , and that the knowledge of this parameter only would be enough to derive a sufficiently accurate model of the OG. Thus, estimating r_0 during closed-loop operation is a crucial step for PyWFS OG tracking. In order to assess the accuracy on r_0 we need to reach, we probe the impact of an error in the estimation of r_0 on the OG computation in figure 8. In this plot, we can see for both configurations studied what is the maximal error that can be tolerated on the estimation of r_0 in order to maintain the error on OG under $\pm 10\%$. In order to stay under $\pm 10\%$ error on the OG, we see that we need to be more accurate for bad seeing regimes and for cases with less actuators in the pupil. Overall, the values presented in this figure show that we don't need an unreachable precision on the Fried parameter to accurately compute the OG using the presented method.

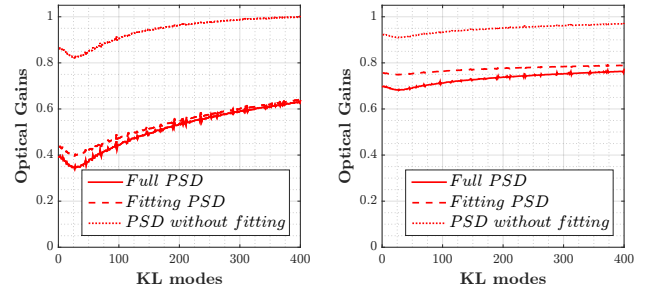


Fig. 7. Contribution of the corrected and non-corrected part of a closed loop PSD ($r_0 = 15\text{ cm}$) to the OG. **Left:** For 20 actuators in the pupil - NAOS configuration. **Right:** For 40 actuators in the pupil - SPHERE configuration.

4. Conclusions

The work presented here proposes a new method to compute PyWFS OG. Our technique relies on a physical description of the wavefront sensor through a convolutional model, which allows to analytically compute the impact of residual phases on PyWFS measurements. We demonstrated the accuracy of this method through a comparison with End-to-End simulations for different system configurations.

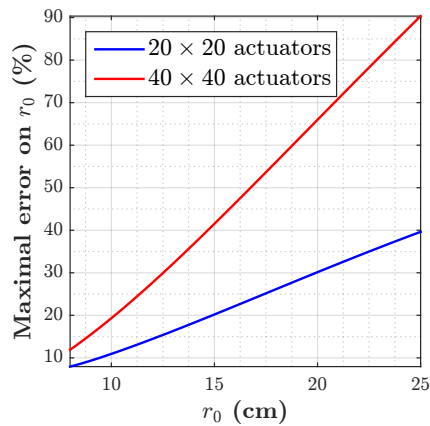


Fig. 8. Maximum acceptable error (in percent) on the estimation of r_0 to ensure an error on the computed OG under $\pm 10\%$ for two system configurations.

Our method requires the knowledge of the residual phases statistical characteristics to compute the OG. We presented here a practical solution to estimate the statistics of the residual phases using the telemetry data of the AO loop, as it is done in the PSF reconstruction field. We showed that the most important piece of information is the knowledge of the turbulence strength through the Fried parameter r_0 . We also showed that from this r_0 parameter alone, a good approximation of the OG could be done. In other words, any AO-pyramid system that would provide an online estimation of r_0 could benefit from an estimation of its OG. This work can also be applied to any kind of Fourier-filtering wavefront sensor and provides a new insight on Fourier Filtering WFS OG and how to manage them.

Acknowledgments

This document has been prepared as part of the activities of OPTICON H2020 (2017-2020) Work Package 1 (Calibration and test tools for adaptive-optics assisted E-ELT instruments). OPTICON is supported by the Horizon 2020 Framework Programme of the European Commission's (Grant number 730890). This work was supported by the Action Spécifique Haute Résolution Angulaire (ASHRA) of CNRS/INSU co-funded by CNES. This work also benefited from the support of the WOLF project ANR-18-CE31-0018 of the French National Research Agency (ANR).

References

- Beltramo-Martin, O., Correia, C. M., Ragland, S., et al. 2019, *Monthly Notices of the Royal Astronomical Society*, 487, 5450–5462
- Beuzit, J. L., Vigan, A., Mouillet, D., et al. 2019, *A&A*, 631, A155
- Conan, R. & Correia, C. 2014, in , 91486C
- Davies, R., Alves, J., Clénet, Y., et al. 2018, *The MICADO first light imager for the ELT: overview, operation, simulation*
- Deo, V., Gendron, É., Rousset, G., et al. 2019, *A&A*, 629, A107
- Deo, V., Rozel, M., Bertrou-Cantou, A., et al. 2019
- Esposito, S., Pinna, E., Puglisi, A., et al. 2015in
- Fauvarque, O., Janin-Potiron, P., Correia, C., et al. 2019, *J. Opt. Soc. Am. A*, 36, 1241
- Fétick, R. J. L., Fusco, T., Neichel, B., et al. 2019, *A&A*, 628, A99
- Guyon, O. 2005, *The Astrophysical Journal*, 629, 592–614
- Hutterer, V., Ramlau, R., & Shatokhina, I. 2018, *Real-time Adaptive Optics with pyramid wavefront sensors: A theoretical analysis of the pyramid sensor model*
- Korkiakoski, V., Véridaud, C., & Louarn, M. L. 2008, in *Adaptive Optics Systems*, ed. N. Hubin, C. E. Max, & P. L. Wizinowich, Vol. 7015, International Society for Optics and Photonics (SPIE), 1422 – 1431

- Meimon, S., Petit, C., & Fusco, T. 2015, *Optics Express*, 23, 27134
- Neichel, B., Fusco, T., Sauvage, J.-F., et al. 2016, in *Astronomical Telescopes + Instrumentation*
- Ragazzoni, R. 1996, *Journal of Modern Optics*, 43, 289
- Rigaut, F. J., Veran, J.-P., & Lai, O. 1998, in *Adaptive Optical System Technologies*, ed. D. Bonaccini & R. K. Tyson, Vol. 3353, International Society for Optics and Photonics (SPIE), 1038 – 1048
- Roddier, F. 1981
- Véridaud, C. 2004, *Optics Communications*, 233, 27

-
- ¹ Aix Marseille Univ, CNRS, CNES, LAM, Marseille, France
e-mail: vincent.chambouleyron@lam.fr
- ² ONERA The French Aerospace Laboratory, F-92322 Châtillon, France
- ³ IFREMER, Laboratoire Detection, Capteurs et Mesures (LDCM), Centre Bretagne, ZI de la Pointe du Diable, CS 10070, 29280, Plouzane, France
- ⁴ W. M. Keck Observatory, 65 - 1120 Mamalahoa Hwy., Kamuela, HI 96743, USA
- ⁵ UK Astronomy Technology Centre, Blackford Hill, Edinburgh EH9 3HJ, United Kingdom